The Two-Dimensional Ising Model: A Numerical Simulation

Luke Mozarsky
Department of Physics, Columbia University, New York, NY
(Dated: December 18, 2024)

Phase transitions in physical systems can often be described by simplified lattice models that rely on basic interactions between neighboring lattice sites. These models can identify macroscopic critical behaviors, which are universal to systems possessing the same inherent symmetries. We present a simulation of the two-dimensional Ising model on a square lattice of side lengths $L = 10, 16, 24$, and 36. This simulation confirms many of the theoretically calculated critical exponents that govern paramagnetic-ferromagnetic phase transitions in two dimensions, as well as the critical temperature T_C at which the transition occurs.

I. INTRODUCTION

Physical systems that undergo magnetic phase transitions can often be described with a simple model consisting of a lattice array governed by nearest-neighbor interactions. The Ising model is a toy model that can be used to describe systems that undergo a continuous paramagnetic-ferromagnetic phase transition. While the Ising model is not a realistic microscopic of magnetism, certain behaviors of magnetic materials near the phase transition are independent of the microscopic properties of the Hamiltonian. This phenomenon, aptly named *critical universality*, allows us to determine the scaling behavior of thermodynamic quantities near the critical temperature T_C of the transition for *any* system of the same dimension that experiences the same symmetry-breaking, regardless of microscopic properties.

The Ising model Hamiltonian is given by

$$H = -J\sum_{\langle ij\rangle}\sigma_i\sigma_j - \mu_B B\sum_i \sigma_i \tag{1}$$

where $\sigma_i \in \{+1, -1\}$ is the spin of lattice i, B, is an applied magnetic field, μ_B is the magnetic moment of each lattice site, the symbol $\langle ij\rangle$ represents a summation over nearest neighbor pairs, and J is a parameter representing the strength of interaction between nearest neighbors. With $B = 0$, Eq. 1 becomes

$$H = -J\sum_{\langle ij\rangle}\sigma_i\sigma_j. \tag{2}$$

For $J > 0$ ($J < 0$) the lattice sites tend to be aligned (anti-aligned) representing a tendency to form ferromagnetic (anti-ferromagnetic) states.

In this work, we simulate the $d = 2$ dimensional Ising model via a square lattice with side length L and total number of lattice sites $N = L^2$. By setting $B = 0$ and $J = 1$, we expect to observe a transition from paramagnetic states above some critical temperature T_C to ferromagnetic states below this critical temperature. Fig. 1 visualizes several lattice configurations simulated in this work.

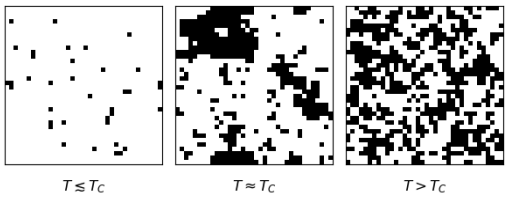

FIG. 1. Convergent configurations of the 2D Ising model designed in this work, at different temperatures.

For $T > T_C$ (right), lattice spins are more or less randomly oriented, demonstrating the low-order / high-symmetry phase of the system. Near T_C (middle), groups of correlated spins arise, leading to a more ordered configuration. For $T < T_C$, all or nearly all lattice sites are aligned; the $\mathbb{Z}_2$ symmetry of the system has been broken, and the lattice is in a ferromagnetic phase. The theoretically predicted critical temperature in the two-dimensional Ising model is

$$T = \frac{2}{\ln(1+\sqrt{2})} \approx 2.269 \tag{3}$$

in units of J/k_B.

II. NUMERICAL SIMULATIONS

A. Numerical approximation of the probability density

We are interested in studying how thermodynamic quantities of the system vary near T_C. We can compute the statistical expectation value of a physical quantity X on the lattice as

$$\langle X\rangle = \sum_\nu P_\nu X(\nu) \tag{4}$$

where $X(\nu)$ is the quantity evaluated on the configuration labeled by ν and

$$P_\nu = \frac{1}{Z}e^{-\beta E_\nu} \tag{5}$$

is the Boltzmann probability density for the configuration. The partition function, Z, is a normalization factor, defined as the sum of Boltzmann factors of all configurations:

$$Z = \sum_{\nu} e^{-\beta E_\nu}. \tag{6}$$

It then becomes clear that P_ν is subject to the constraint

$$\sum_{\nu} P_\nu = 1 \tag{7}$$

which is obviously true given that P_ν is a probability density.

For the Ising model, a configuration ν represents a unique arrangement of spins $\{\sigma_i\}$. It becomes clear that to compute the partition function exactly we would need to generate an immense number of configurations: for a lattice of dimension L, we must sum over 2^{L^2} configurations. A relatively small choice is $L = 10$, which results in $2^{100} \sim 10^{30}$ configurations.

To overcome this problem, one solution is to devise a way of sampling configurations such that after many samples our distribution of selected configurations approximates that of Eq. 5. To do so, we introduce the "master equation" that describes the evolution of the probability density as a function of time,

$$\frac{dP_\nu(t)}{dt} = \sum_{\sigma} \left(P_\sigma(t)W(\sigma \to \nu) - P_\nu(t)W(\nu \to \sigma)\right), \tag{8}$$

where $P_\nu(t)$ is the probability of the system having configuration ν at time t and $W(\sigma \to \nu)$ is the probability per unit time of the system transitioning from configuration σ to configuration ν. In light of this, we can view this equation as describing the rate at which the system enters or exits the configuration ν: the first term on the right-hand side represents the rate at which the configuration ν is populated, while the second term represents the rate at which the configuration ν is depopulated.

We further introduce a constraint on Eq. 8. The system in configuration ν must transition to some configuration, meaning that

$$\sum_{\sigma} W(\nu \to \sigma) = 1 \tag{9}$$

where the summation over σ includes the existing configuration ν. (The system may stay in its current configuration, but not for all t.) Note that the constraint given in Eq. 7 still applies here.

In the limit that P_ν does not change in time, that is $dP_\nu(t)/dt = 0$, we have

$$\sum_{\sigma} P_\sigma W(\sigma \to \nu) = \sum_{\sigma} P_\nu W(\nu \to \sigma) \tag{10}$$

where the right-hand side is simply P_ν by virtue of the constraint in Eq. 9. Thus, by choosing transition probabilities $W(\nu \to \sigma)$ and $W(\sigma \to \nu)$ such that Eq. 10 is satisfied, we are guaranteed to recover the desired probability density. We can avoid the complex summation on the left-hand side by requiring

$$P_\sigma W(\sigma \to \nu) = P_\nu W(\nu \to \sigma) \tag{11}$$

which is known as the condition of detailed balance. Clearly Eq. 10 is satisfied if this condition is met. Given we are working with Boltzmann probability densities, this yields a constraint on the transition probabilities, such that

$$\frac{W(\nu \to \sigma)}{W(\sigma \to \nu)} = \frac{P_\sigma}{P_\nu} = e^{-\beta(E_\sigma - E_\nu)}. \tag{12}$$

B. Metropolis algorithm

One particular choice of transition probabilities is

$$W(\nu \to \sigma) = \begin{cases} 1 & P_\sigma \geq P_\nu \ (E_\sigma \leq E_\nu) \\ \frac{P_\sigma}{P_\nu} & P_\sigma < P_\nu \ (E_\sigma > E_\nu) \end{cases} \tag{13}$$

which defines the *Metropolis algorithm*. Practically, this can be implemented as follows: for a system in a configuration ν, if the probability weight (the Boltzmann factor) of a new, randomly chosen configuration with energy E_σ is greater than the Boltzmann factor of the current configuration with energy E_ν, we always transition the system to the new configuration. Otherwise, we transition to the new configuration with probability P_σ/P_ν. This second scenario is crucial; if we always transitioned to the configuration with the lowest energy, the algorithm would be deterministic, and we would not get a good estimate over the Boltzmann density. By transitioning to a configuration with a greater total energy with some probability less than unity, given enough transitions, we will explore the full distribution of configurations.

The proof that the Metropolis algorithm satisfies detailed balance (Eq. 11) is straightforward. For clarity, let i denote the current configuration and let f denote a randomly sampled configuration. The first case is when $P_f \geq P_i$. In this case, Eq. 13 dictates that $W(i \to f) = 1$ and $W(f \to i) = P_i/P_f$. Thus we have

$$P_f W(f \to i) = P_f \frac{P_i}{P_f} = P_i = P_i W(i \to f).$$

Next, we consider the case where $P_f < P_i$. In this case, Eq. 13 demands that $W(i \to f) = P_f/P_i$ and $W(f \to i) = 1$. Now we have

$$P_f W(f \to i) = P_f = P_i \frac{P_f}{P_i} = P_i W(i \to f)$$

and thus detailed balance is satisfied in both cases.

III. ISING MODEL SIMULATION

A. Parameters and thermodynamic quantities

In this work, we simulate lattices of dimension $L = 10$, 16, 24, and 36, yielding the number of sites to be $N = L^2 = 100$, 256, 576, and 1296, respectively. For each system size, we run a simulation at 300 temperatures, from $T = 0.015$ to $T = 4.5$ in steps of 0.015. A single simulation consists of "sweeping" across the lattice and, for each site, applying the Metropolis algorithm. This means that for a given site, we calculate the energy of the configuration with said site's spin flipped; if the energy of this new configuration is less than the current configuration, we flip the spin (as dictated by Eq. 13). Otherwise, we only flip the spin with probability $e^{-\beta\Delta E}$, where ΔE is the difference in the energy of the new and old configurations. With $J = 1$, it is not hard to see that at a given lattice site (i, j),

$$\Delta E = 2\sigma_{i,j}\left(\sigma_{i+1,j} + \sigma_{i-1,j} + \sigma_{i,j+1} + \sigma_{i,j-1}\right). \quad (14)$$

This is to say that if the transition is made, the change in energy of the configuration is two times the product between the spin of the given site and the sum of the spins of its nearest neighbors. This relation makes it computationally simple to apply the metropolis algorithm repeatedly over the lattice. We define a single "sweep" as a decision to flip or keep the spin of each site on the lattice; we perform 10^5 sweeps to thermalize the lattice, and then we execute 3×10^5 sweeps over which we measure certain thermodynamic quantities.

The thermodynamic quantities of interest are the average total energy $E = \langle H \rangle$, the specific heat

$$C = \frac{1}{Nk_BT^2}\left(\langle H^2\rangle - \langle H\rangle^2\right), \quad (15)$$

the magnetization per site $M = \langle \sigma_i \rangle$ and the magnetic susceptibility

$$\chi = \frac{N}{k_BT}\left(\langle \frac{1}{N}\left|\sum \sigma_i\right|^2\rangle - \langle \sigma_i\rangle^2\right). \quad (16)$$

Notice that by setting $J = 1$, energies will be measured in units of J. This implies that temperature will be measured in units of J/k_B and that entropy and specific heat will be measured in units of k_B.

B. Results

In Fig. 2 we plot the average energy per site as a function of the temperature. We notice that at low temperatures the energy is minimized, reflecting the system's tendency to align its spins. At high temperatures, the opposite is true: the lattice spins tend to be randomly oriented and hence the energy is maximized. At an intermediate temperature between $T = 2$ and $T = 3$ there is a steep change in the energy, which is a sign of a phase transition. This is in line with the expected phase transition from paramagnet to ferromagnet states that occurs at the theoretically calculated critical temperature of $T_C \approx 2.269$.

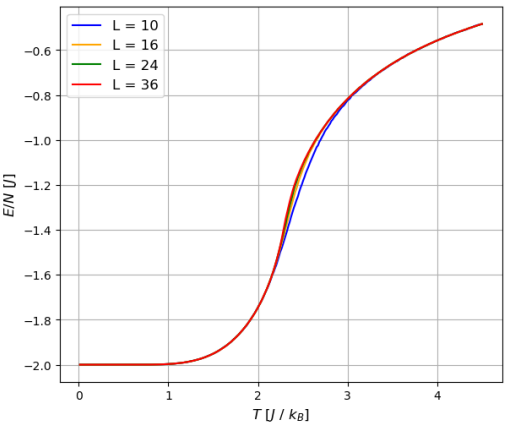

FIG. 2. Average energy per lattice site E/N as a function of temperature for the four system sizes simulated.

Fig. 3 shows the magnetic susceptibility as a function of temperature for each system size. We note that the peak susceptibility increases with L but that for each system the peak occurs around a common temperature. These temperatures are $T_C(L = 10) \approx 2.475$, $T_C(L = 16) \approx 2.400$, $T_C(L = 24) \approx 2.355$, and $T_C(L = 36) \approx 2.325$, which are all in line with the expected critical temperature. One may recognize that the critical temperature in each system appears to decrease with the system size. This is expected, and for the two-dimensional Ising model the critical temperature recovered in a system of dimension L is expected to scale as

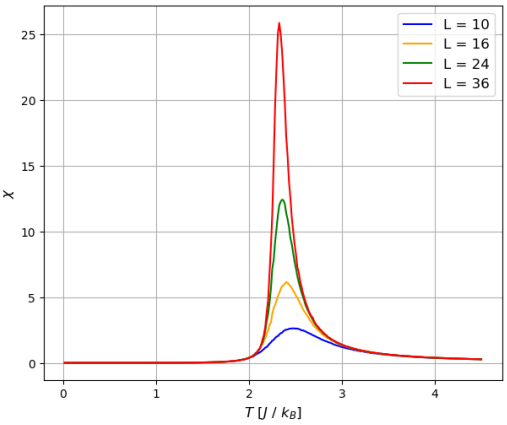

FIG. 3. Magnetic susceptibility χ as a function of temperature for the four systems simulated.

$$T_C(L) = T_C + (x_0T_C)L^{-1/\nu} \quad (17)$$

where T_C is the true critical temperature (Eq. 3). The exponent ν is the critical exponent that governs the divergence of the correlation length near the critical temperature; we take $\nu = 1$, the exact value for the two-dimensional Ising model, hence $L^{-1/\nu} = L^{-1}$.

Fig. 4 plots $T_C(L)$ (derived from the peak values of the magnetic susceptibility) as a function of L^{-1}. The green

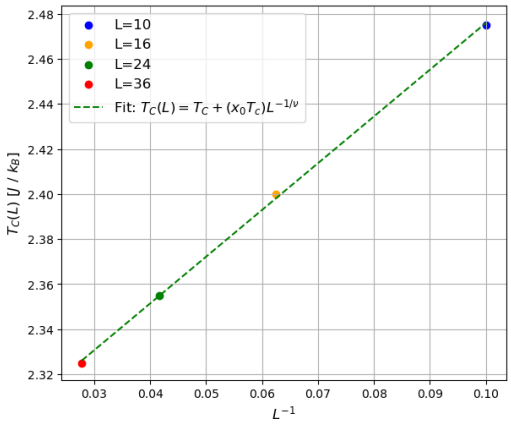

FIG. 4. Critical temperature $T_C(L)$ as determined from the peak magnetic susceptibility for each system size, as a function of L^{-1}. The green dashed line represents a fit of Eq. 17 to the data.

dashed line represents a fit of Eq. 17 to the four data points. For our purposes, we take x_0 to be a parameter of the fit. The fit yields $T_C \approx 2.268$, in high agreement with the exact value.

We also recover the critical exponent γ, which dictates the divergence of the magnetic susceptibility near the critical point:

$$\chi \sim (\pm t)^{-\gamma}, \quad t \equiv \frac{T - T_C}{T_C}. \tag{18}$$

We should find that

$$\chi(T_C(L)) \propto L^{\gamma/\nu} \tag{19}$$

where $\chi(T_C(L))$ is the value of the magnetic susceptibility at the critical temperature recovered for a system of dimension L. This implies that the slope of a linear fit to these data on a log-log scale should be γ/ν. In Fig. 5 we plot $\chi(T_C(L))$ as a function of L on a log-log scale. We recover $\gamma/\nu \approx 1.781$, which is $\sim 1.8\%$ from the exact value of $\gamma/\nu = 1.75$.

In Fig. 6 we plot the scaled magnetic susceptibility $L^{-\gamma/\nu}\chi$ as a function of the scaling variable $L^{1/\nu}(T - T_C(L))$. We should find that

$$L^{-\gamma/\nu}\chi(T) \propto f(L^{1/\nu}(T - T_C(L))) \tag{20}$$

where f is some function of the scaling variable. This is to say that the susceptibility curves for each system size should collapse onto a single curve in the vicinity

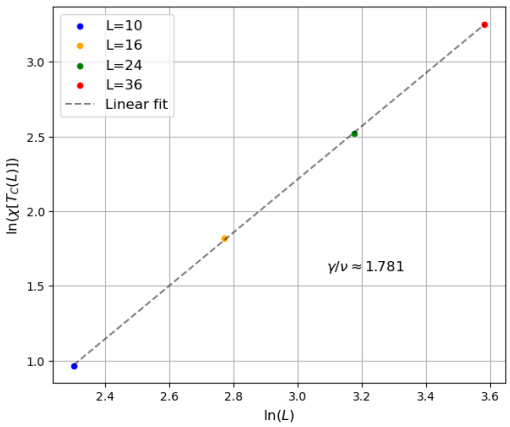

FIG. 5. Peak magnetic susceptibility $\chi(T_C(L))$ as a function of the lattice dimension L, on a log-log scale. The grey dashed line is a linear fit to the data.

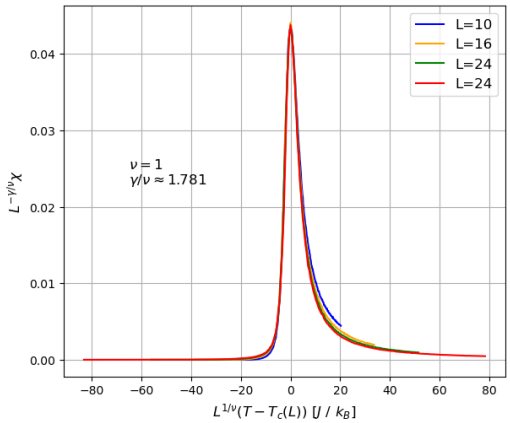

FIG. 6. Scaled magnetic susceptibility $L^{-\gamma/\nu}\chi$ as a function of the scaling variable $L^{1/\nu}(T - T_C(L))$. The exact $\nu = 1$ and fit-extracted $\gamma/\nu = 1.781$ are used here.

of the critical temperature; Fig. 6 clearly shows this phenomenon.

In Fig. 7 we plot the average site magnetization M as a function of the temperature. Notice that as the system size increases, the sharpness of the change from paramagnetic to ferromagnetic phases also increases. This is evident of finite-size effects, where the critical phenomena are smeared out as the correlation length approaches the lattice size L.

In Fig. 8 we again verify the relation in Eq. 19 but for the magnetization rather than the magnetic susceptibility. By plotting $L^{\beta/\nu}M$ as a function of temperature, we expect to see the magnetization curves for each system size intersect at the critical temperature. In this case, β is the critical exponent that governs the behavior of the order parameter M near the critical temperature:

$$M \propto (-t)^{\beta} \quad \text{for } t \to 0^-. \tag{21}$$

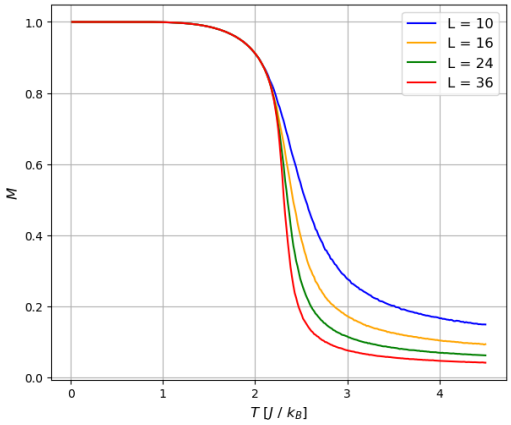

FIG. 7. Magnetization per lattice site M as a function of temperature.

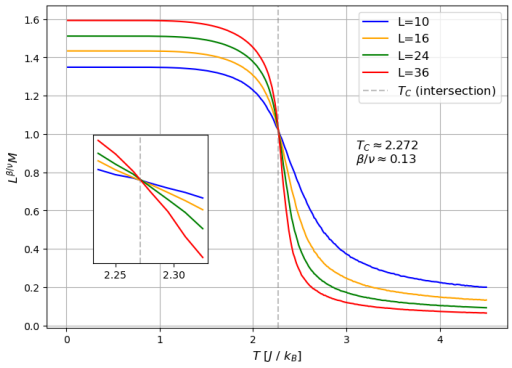

FIG. 8. Scaled magnetism $L^{\beta/\nu}M$ as a function of temperature. The exponent $\beta/\nu = 0.13$ was chosen to yield the closest intersection of all curves for different system sizes.

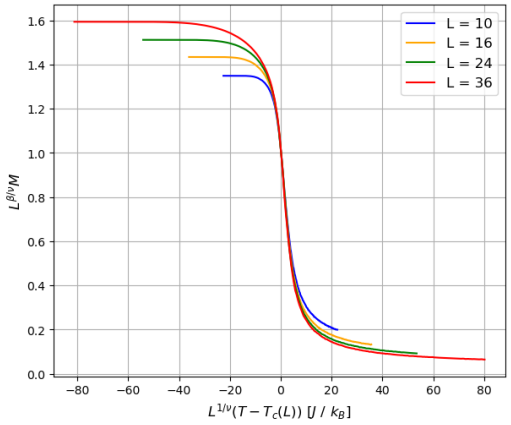

FIG. 9. Scaled magnetism $L^{\beta/\nu}M$ as a function of the scaling variable $L^{1/\nu}(T - T_C(L))$. The exact $\nu = 1$ is used here, and $\beta/\nu = 0.13$ is taken from Fig. 8.

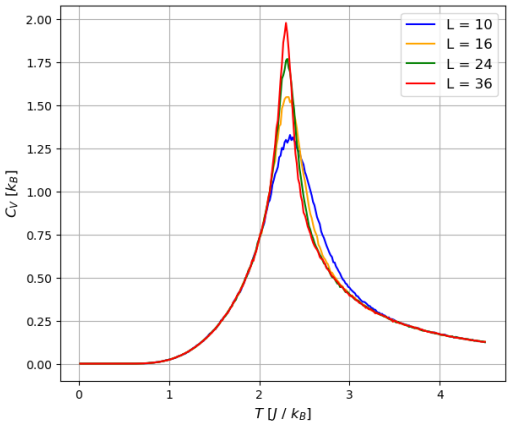

FIG. 10. Specific heat C_V as a function of temperature for each of the lattice sizes simulated.

We take $\beta/\nu = 0.13$ which is the value that provides the best intersection between the four curves. The curves intersect at $T \approx 2.272$, again in strong agreement with the exact value.

In Fig. 9 we plot $L^{\beta/\nu}M$ as a function of the scaling variable $L^{1/\nu}(T - T_C)$. As dictated by Eq. 20 (with $\chi \to M$ and $-\gamma \to \beta$) we expect to see the magnetization curves collapse on each other in the vicinity of the critical temperature, which we do. Note that although we took $\beta/\nu = 0.13$ which deviates significantly from the exact value of $\beta/\nu = 0.25$, the plot in Fig. 9 is nearly identical regardless of which of the two values we choose.

Next we analyze the specific heat of the system. In Fig. 10 we show the specific heat as a function of temperature for the four lattice sizes. The critical temperature in each system size $T'_C(L)$ as well as the value of the maximal specific heat $C_{\max}(L)$ vary from lattice to lattice, but similar finite-size scaling relationships can be used to account for these effects. We note that $(T'_C(L), C_{\max}(L)) = (2.340, 1.329)$ for $L = 10$, $(2.310, 1.549)$ for $L = 16$, $(2.310, 1.771)$ for $L = 24$, and $(2.295, 1.979)$ for $L = 36$.

Fig. 11 shows $T'_C(L)$ as a function of L^{-1}. The grey dashed line represents a fit of Eq. 17 to the data. While the linear relationship is not as well defined for the specific heat as it is for the magnetic susceptibility, we still recover a thermodynamic critical temperature of $T_C \approx 2.280$, just slightly deviating from the exact value.

For the two-dimensional Ising model, the critical parameter α describing the divergence of the specific heat near the critical temperature is zero. This implies that the specific heat diverges logarithmically with the *lattice size* L near the transition. We confirm this in Fig. 12 where we plot $C_{\max}$ as a function of $\ln L$. The clear linear relationship indicates that the specific heat does indeed evolve logarithmically with L.

We also explore the behavior of the entropy of the system. The specific heat yields a relationship for the en-

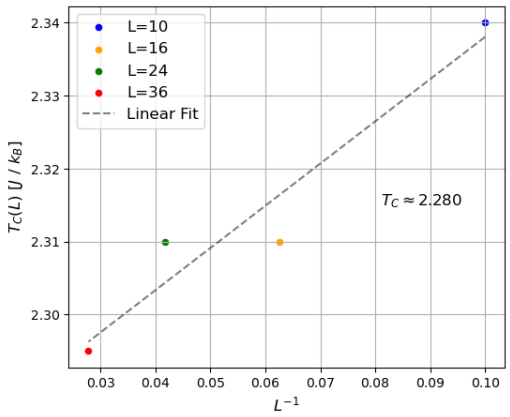

FIG. 11. Critical temperature $T_C(L)$ as determined from the peak specific heat for each system size, as a function of L^{-1}. The grey dashed line represents a fit of Eq. 17 to the data.

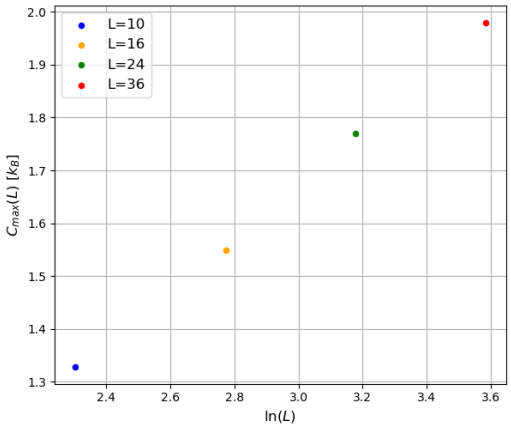

FIG. 12. Peak specific heat $C_{\max}(L)$ as a function of the logarithm of the lattice size $\ln(L)$.

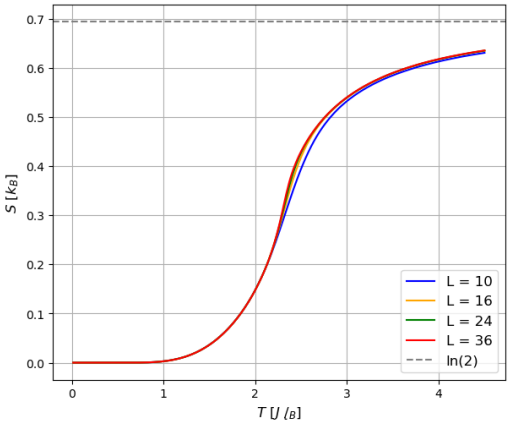

FIG. 13. Entropy S as a function of temperature. The grey dashed line represents $S = \ln(2) \approx 0.693$.

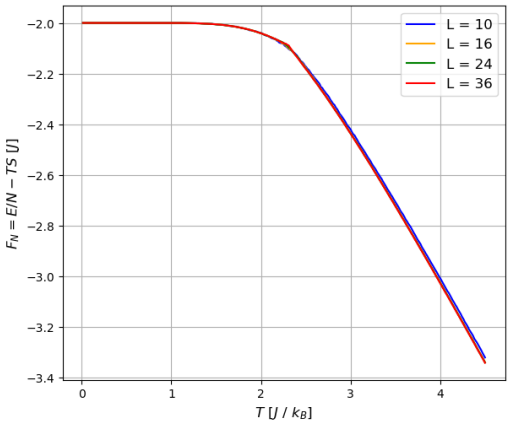

FIG. 14. Free energy per particle F as a function of temperature.

tropy per lattice site:

$$S(T) = \int_0^T dT' \frac{C(T')}{T'}. \tag{22}$$

For the Ising model we expect $S(T \to \infty) = \ln 2 \approx 0.693$. In Fig. 13 we confirm this expectation by numerically integrating the specific heat as a function of temperature. At the maximum temperature $T = 4.5$ explored in this work, we find $S(T = 4.5) \approx 0.6303$, 0.6345, 0.6347, and 0.6351 for lattice sizes of $L = 10$, 16, 24 and 36, respectively. Due to the finite size of the lattice, the entropy per site still lies somewhat below ln2, but it is clear that as $N \to \infty$ the entropy is expected to approach ln2 asymptotically.

Finally, we calculate the free energy per site

$$F = E/N - TS \tag{23}$$

and plot it as a function of temperature in Fig. 14. In the region where the second term in Eq. 23 dominates (high temperature regime), the free energy behaves as expected, with a linear slope of $\sim \ln 2$. This is evidence of the fact that at higher temperatures, thermal fluctuations in the system dominate, contributing to the highly disordered, highly symmetric paramagnetic phase.

IV. CONCLUSION

In this work, we confirmed many of the critical phenomena associated with two-dimensional paramagnetic-ferromagnetic phase transitions by simulating the Ising model. These critical phenomena are universal for two-dimensional systems possessing the same $\mathbb{Z}_2$ symmetry breaking, and do not rely on the microscopic properties of the Hamiltonian governing the system. Thus, this study confirms behaviors that can characterize realistic phase transitions in physical systems when taken in the ther-

modynamic limit.

ACKNOWLEDGMENTS

I would like to thank you, Professor Ochoa, for a great semester. I want to especially mention that your notes were extremely helpful in reinforcing the material over the past several months. I hope to be able to apply some of the things I've learned about phase transitions to my research field of experimental heavy-ion physics.

Also, I would like to thank Alejandro for his tremendous efforts as course TA. His recitations were excellent and focused on solving problems central to the course material.